Temporal photonic (time) crystal with a square profile of both permittivity $\varepsilon(t)$ and permeability $\mu(t)$

José Gabriel Gaxiola-Luna *, and P. Halevi †
Instituto Nacional de Astrofísica, Óptica y Electrónica, Tonantzintla, 72840 Puebla, Mexico

(Received 6 September 2019; accepted 2 April 2021; published 22 April 2021)

We present a comprehensive study of a "temporal photonic crystal" or "time crystal" with a square profile of both its permittivity $\varepsilon(t)$ and permeability $\mu(t)$. The continuity of the displacement field $D(t)e^{ikx}$ and magnetic field $B(t)e^{ikx}$(where k is the wave number) across the (simultaneous) discontinuities of $\varepsilon(t)$ and $\mu(t)$ facilitates the Krönig-Penney methodology of Solid State physics, leading to an analytic photonic band structure (PBS) that relates the wave frequency ω to k. It is periodic in ω, with the period given by the modulation frequency Ω and exhibits k bands separated by k gaps. The PBS depends qualitatively on three parameters: the strengths of the electric and magnetic modulations m_ε and m_μ and $\tau = t_1/(t_1 + t_2)$ associated with the intervals t_1 and t_2 that comprise a modulation period $T(= 2\pi/\Omega)$. For equal electric and magnetic modulations the PBS is composed of straight lines and there are no k gaps. This can be explained by the fact that for $m_\varepsilon = m_\mu$ the wave impedance is continuous at the abrupt interfaces of $\varepsilon(t)$ and $\mu(t)$; hence no reflections occur. Conversely, the existence of gaps for $m_\varepsilon \neq m_\mu$ can then be associated with diffraction occurring for the frequencies $\omega = (n/2)\Omega$ in the presence of discontinuities of the wave impedance. In comparison to harmonic modulation, where only the first gap is appreciable, for square modulation large gaps, that increase with the difference $|m_\varepsilon - m_\mu|$, exist even between distant bands. In the particular case $m_\mu = -m_\varepsilon$ [with $\varepsilon(t)$ and $\mu(t)$ oscillating out of phase], all the gaps have equal widths. The field $D(t)$ displays the Bloch-Floquet behavior, namely, oscillations of frequency Ω being modulated by an envelope of frequency $\omega(< \Omega)$. For $\omega = (n/2)\Omega$, the fields are standing waves. We also studied the optical response to a monochromatic wave incident at the modulated slab, namely, the spectral behavior of the frequency combs that are transmitted and reflected by the slab, as well as the field profile inside the slab. Especially interesting is the case of equal modulations $m_\varepsilon = m_\mu$ where only the fundamental harmonic $n = 0$ is transmitted if the modulations are out of phase, while no light at all is reflected if they are in phase.

DOI: 10.1103/PhysRevB.103.144306

I. INTRODUCTION

We study propagation of a plane light wave in a magnetodielectric medium with time-dependent permittivity $\varepsilon(t)$ and permeability $\mu(t)$. While our medium is spatially uniform, $\varepsilon(t)$ and $\mu(t)$ are periodic in time, with simultaneous, abrupt changes, as seen in Fig. 1. The dispersion relation in such a modulated system takes the form of a photonic band structure (PBS), which we seek to analyze in depth, as well as the time-dependence of the EM fields. Our investigation concerns both the infinite medium and a slab and is restricted to stable solutions (characterized by real frequencies ω and wave numbers k).

The interest in such "temporal photonic crystals" or, briefly "time crystals," goes back to F. R. Morgentahler [1] who considered a medium with abrupt change of its refractive index without impedance variations. He demonstrated a change of the electromagnetic wave velocity, conservation of electromagnetic momentum and possibility to increase the energy of the electromagnetic wave. Another early paper, by T.M.Ruiz *et al.* [2], deals with propagation in the presence of an abrupt change of the permittivity and demostrated the conversion of an initial wave into "transmitted" and "reflected" waves by the temporal interface. In spite of an abrupt shift of $\varepsilon(t)$ and $\mu(t)$ the fields $D(t)$ and $B(t)$ remain continuous at the instant of that shift [3,4]. At such a temporal interface the transmitted fields can increase [4–6] because of energy being supplied by the modulated medium to the wave [1]. These calculations were extended by Pacheco-Peña *et al.* [7] to a metallic slab with negative permittivity. For $\varepsilon(t)$ with harmonic periodicity Zurita-Sánchez *et al.* [8] obtained a PBS with k bands separated by wave number k gaps, rather than ω gaps as in case of ordinary (spatial) photonic crystals. As demonstrated by N.Wang *et al.* [9] such behavior holds good even for a complex $\varepsilon(t)$. The WKB approximation [5], the transmission matrix method [10,11], and topological analysis [12,13] have been applied to the case of square (abrupt) modulation of the permittivity, leading to a large number of band gaps in comparison to harmonic modulation. Effects on wave propagation due to modulation of both $\varepsilon(t)$ and $\mu(t)$ were researched by Martínez-Romero *et al.* [14]. Continuous wavelike modulation of the form $\varepsilon(x - vt)$ was also investigated [15–18]. Repercussions of such "spatiotemporal" modulation were covered at length by Caloz and Deck-Léger [3]. For time crystals, the fields are superpositions of harmonic waves with frequencies $|\omega - n\Omega|$, where $\Omega/2\pi$ is the

*gxluna@inaoep.mx
†halevi@inaoep.mx

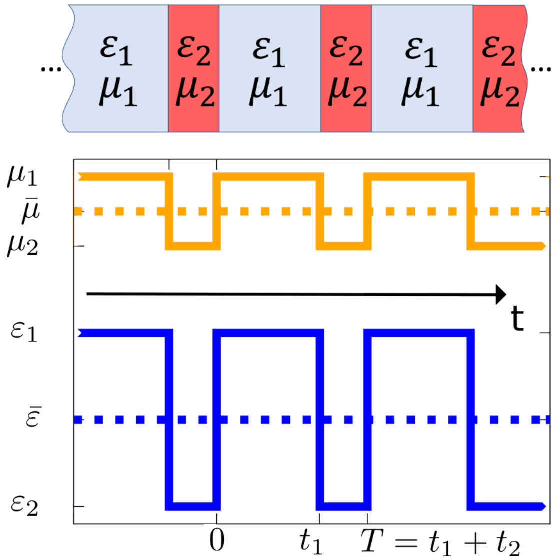

FIG. 1. The permittivity $\varepsilon(t)$ and permeability $\mu(t)$ are periodic functions of time with period T, composed of sections t_1 and t_2. Here $\bar{\varepsilon} = (1/2)(\varepsilon_1 + \varepsilon_2)$ and $\bar{\mu} = (1/2)(\mu_1 + \mu_2)$.

modulation frequency and n runs over all integers; hence, the optical response is manifested as a "frequency comb" [8]. Taravati and Kishk [19] show that in a spatiomodulated slab with equal modulations of the permittivity and permeability there are no reflections at the temporal interfaces, although frequency combs do obtain at the slab surfaces. It was also shown that in such media nonreciprocity with respect to the direction of propagation is obtained [20], with this effect increasing with the modulation strength. Other publications report parametric resonances in time crystals with modulation of the permittivity and/or permeability for specific thicknesses of a modulated slab (that depends on the modulation frequency) [21–23].

Interesting properties found in optical and electronic systems are leading to renewed interest in modulated systems. For example, it was shown that modulation of a medium can change and control the shape of an optical pulse [24–27], nonreciprocal optical systems were designed with no recourse to applied magnetic fields [28,29], and Y.Zhang *et al.* [30] reported that the radiation from an antenna transmitted through a weakly modulated medium can suffer a frequency shift. Now, while it is very difficult in practice to substantially modulate the permittivity or permeability, there exists a close analogy with low pass transmission lines, valid in the long-wavelength limit and negligible dissipation [31–33]. This led to the first observation of a forbidden wave number (phase advance) gap [34]. Nonreciprocal transmission lines for the "front end" were designed using varactors modulated by a pump wave [35–37]. Employing modulated varactors, low noise parametric amplifiers were also designed [38]. Miscellaneous applications, based on space-time modulation, were designed: a mixer-duplexer-antenna leaky-wave system [39] and frequency mixing [40] for aperiodic modulation. It was also demonstrated that the Bode-Fano limit can be extended for short pulses by abrupt switching of the impedance transmission line [41]. The accumulation of energy in reactive elements has been recently found to have potential for the design of parametric oscillators [42]. The harmonics generated in a weakly modulated spatiotemporal transmission line conserve energy according to the Manley-Rowe relation [39]. We also note that the accumulation of energy in time-modulated systems could lead to sustained growth of an emitted signal; for this reason an analysis of stability, based on the transition function of the system was developed [10,43].

The square modulations of Fig. 1 are ideally suited for the Krönig-Penney methodology (KPM), introduced by these scientists in 1931 to obtain a first quantum-mechanical band structure of a crystal [44]. While it was a toy model as far as real crystals are concerned, it showed the way for more sophisticated metods. The constant sections have simple, well known solutions that have to be connected by appropriate boundary conditions; in additon, the periodicity is introduced by means of the phase advance over a single period. The KPM has been also implemented for several superlattices: of semiconductors [45], metal-dielectric [46], and semiconductor-graphene [47]. Improvement of the thermogenerating efficiency of a semiconductor superlattice was also reported [48]. Moreover, a similar methodology was used theoretically and experimentally to treat random changes of the dielectric layers [49]. The KPM also led to an interpretation of PBS in terms of reflection and transmission coefficients [50] and to PBSs of alternated plasma and dielectric layers [51–53]. Further, this methodology was employed to layers with nonlinear response, giving rise to solitons in 1D [54] and 2D [55] periodic structures. In addition, propagation through parallel plate [56] and circular waveguides [57] with Krönig-Penney morphology was also studied for application as filter.

In the next section, we will demonstrate the KPM by applying it to the problem of double square modulations of the parameters in Fig. 1: both the permittivity and the permeability; an analitic PBS or dispersion relation $\omega(k)$ will be derived. In Sec. III, we will limit the generality to equal sections t_1 and t_2 in Fig. 1 and will provide graphical results for both the eigenvalues $\omega(k)$ and the eigenfunctions $D(t)$ and $E(t)$. We will consider both different and equal electric modulation strengths and, in the latter case, out-of-phase, and in-phase modulations, see Secs. III A, III B, and III C, respectively. In Sec. IV, we deal with unequal sections t_1 and t_2 in Fig. 1. Simple analytic expressions are derived throughout. Section V is devoted to the optical response of a temporal photonic crystal slab to an incident monochromatic wave. All the fields are described in terms of real frequencies ω and real wave numbers k, thus corresponding to stable solutions, as proved in Appendix using the transition matrix method. The paper concludes in Sec. VI.

II. PHOTONIC BAND STRUCTURE (PBS) AND ELECTROMAGNETIC FIELDS

As shown in Fig. 1, the modulation periods T (and, therefore, modulation frequencies $\Omega/2\pi = 1/T$) of the permittivity $\varepsilon(t)$ and permeability $\mu(t)$ are assumed to coincide. Within every period T there are two intervals of time, t_1 and t_2 (with $t_1 + t_2 = T$) during which both parameters maintain constant values; these are connected by discontinuous rises or falls that occur simultaneously for $\varepsilon(t)$ and $\mu(t)$ at all the instants $t = nT$ and $t = t_1 + nT$ (n assumes all the integer values). However, the two functions can oscillate in phase (as in the example of the figure) or out of phase; we define them for a single period $0 < t < T$ as

$$\varepsilon(t) = \begin{cases} \varepsilon_1 = \bar{\varepsilon}(1 + m_\varepsilon), & 0 < t < t_1 \\ \varepsilon_2 = \bar{\varepsilon}(1 - m_\varepsilon), & t_1 < t < T \end{cases}, \tag{1}$$

$$\mu(t) = \begin{cases} \mu_1 = \bar{\mu}(1 + m_\mu), & 0 < t < t_1 \\ \mu_2 = \bar{\mu}(1 - m_\mu), & t_1 < t < T \end{cases}. \tag{2}$$

Here, $\bar{\varepsilon}$ and $\bar{\mu}$ are simple averages of, respectively, ε_1 and ε_2 and of μ_1 and μ_2 (even if $t_1 \neq t_2$) and the modulation strengths are

$$m_\varepsilon = (\varepsilon_1 - \varepsilon_2)/(\varepsilon_1 + \varepsilon_2), \quad m_\mu = (\mu_1 - \mu_2)/(\mu_1 + \mu_2).$$

While our treatment is limited to positive values of $\varepsilon_{1,2}$ and of $\mu_{1,2}$, the modulations can assume any value in the interval $[-1, 1]$. If the maximum values of both $\varepsilon(t)$ and $\mu(t)$ occur in the same time intervals (as, for instance, in Fig. 1), then both m_ε and m_μ can be taken to be in the interval $[0, 1]$. On the other hand, if it is the maximum values of $\varepsilon(t)$ and minimum values of $\mu(t)$ (and vice versa) that fall in the same intervals then m_ε and m_μ differ in signs; we will choose m_ε in the interval $[0, 1]$ and m_μ in the interval $[-1, 0]$.

Our dynamic medium is assumed to be free of charges and currents, spatially uniform, and isotropic. Then the Faraday and Maxwell laws read as

$$\partial E(x,t)/\partial x = -\partial B(x,t)/\partial t, \tag{3}$$

$$\partial H(x,t)/\partial x = -\partial D(x,t)/\partial t, \tag{4}$$

where $D(t) = \varepsilon(t)E(t)$ and $B(t) = \mu(t)H(t)$. Eliminating the magnetic field, we get a wave equation for the displacement $D(t)$:

$$\frac{\partial^2 D(x,t)}{\partial x^2} = \varepsilon(t)\frac{\partial}{\partial t}\left[\mu(t)\frac{\partial D(x,t)}{\partial t}\right]. \tag{5}$$

This allows a plane wave solution, characterized by a wave number k:

$$D(x,t) = D(t)e^{ikx}. \tag{6}$$

This leaves us with a second-order differential equation for the time-dependent amplitude $D(t)$,

$$\epsilon(t)\frac{\partial}{\partial t}\left[\mu(t)\frac{\partial}{\partial t}(D(t))\right] + k^2 D(t) = 0. \tag{7}$$

Taking advantage of the fact that $\varepsilon(t)$ and $\mu(t)$ are constant within the intervals $0 < t < t_1$ and $t_1 < t < T$, the solution must have the form

$$D(t) = \begin{cases} D_1^+ e^{-i\omega_1 t} + D_1^- e^{i\omega_1 t}, & 0 < t < t_1 \\ D_2^+ e^{-i\omega_2 t} + D_2^- e^{i\omega_2 t}, & t_1 < t < T \end{cases}. \tag{8}$$

Substitution in Eq.(7) relates the parameters ω_1 and ω_2 to the wave number k as

$$\omega_1 = k/\sqrt{\varepsilon_1\mu_1}, \quad \omega_2 = k/\sqrt{\varepsilon_2\mu_2}. \tag{9}$$

With Eq. (6) in mind, Eq. (8) describes right- and left-propagating waves of the form $e^{i(kx \mp \omega_{1,2} t)}$.

The Bloch-Floquet theorem allows us to extend the solution Eq. (8) from the time-interval $[0, T]$ to arbitrary instants of time t:

$$D(t + nT) = D(t)e^{-in\omega T}. \tag{10}$$

The "Bloch frequency" ω plays the role of the Bloch wave vector $\mathbf{k}$ in spatially periodic systems and is the same as the excitation frequency in the presence of a source. On the other hand, the frequencies $\omega_{1,2}$ in Eq. (9) merely describe the local (in time) behavior in the intervals $t_{1,2}$.

It follows directly from Eqs. (3) and (4) that the fields $B(t)$ and $D(t)$ must be continuous over an abrupt interface in time t_d (where d stands for "discontinuity"). For the displacement vector, we have

$$D(t_d^-) = D(t_d^+). \tag{11}$$

Also, by Eq. (4), the continuity of $B(t) = \mu(t)H(t)$ implies that

$$\mu(t_d^-)\partial D(t_d^-)/\partial t = \mu(t_d^+)\partial D(t_d^+)/\partial t. \tag{12}$$

Then applying Eq. (11) and Eq. (12) to $t_d = t_1$, using Eq. (8) we get

$$D_1^+ e^{-i\omega_1 t_1} + D_1^- e^{i\omega_1 t_1} = D_2^+ e^{-i\omega_2 t_1} + D_2^- e^{i\omega_2 t_1}, \tag{13}$$

$$\begin{aligned} &\mu_1\omega_1(-D_1^+ e^{-i\omega_1 t_1} + D_1^- e^{i\omega_1 t_1}) \\ &\quad = \mu_2\omega_2(-D_2^+ e^{-i\omega_2 t_1} + D_2^- e^{i\omega_2 t_1}). \end{aligned} \tag{14}$$

Similarly, we also apply Eq. (11) and Eq. (12) at the discontinuities $t_d = 0$ and $t_d = T$. In addition, we have to use Eq. (10) for $t = 0^+$:

$$D(T^-) = D(T^+) = D(0^+)e^{-i\omega T}. \tag{15}$$

Then Eqs. (11) and (12) take the following form at the instant $t_d = T$:

$$(D_1^+ + D_1^-)e^{-i\omega T} = D_2^+ e^{-i\omega_2 T} + D_2^- e^{i\omega_2 T}, \tag{16}$$

$$\mu_1\omega_1(-D_1^+ + D_1^-)e^{-i\omega T}\mu_2\omega_2\big(-D_2^+ e^{-i\omega_2 T} + D_2^- e^{i\omega_2 T}\big). \tag{17}$$

Equations (13), (14), (16), and (17) can be rewritten compactly in matrix form:

$$\begin{pmatrix} e^{-i\omega_1 t_1} & e^{i\omega_1 t_1} & -e^{-i\omega_2 t_1} & -e^{i\omega_2 t_1} \\ -\mu_1\omega_1 e^{-i\omega_1 t_1} & \mu_1\omega_1 e^{i\omega_1 t_1} & \mu_2\omega_2 e^{-i\omega_2 t_1} & -\mu_2\omega_2 e^{i\omega_2 t_1} \\ e^{-i\omega T} & e^{-i\omega T} & -e^{-i\omega_2 T} & -e^{i\omega_2 T} \\ -\mu_1\omega_1 e^{-i\omega T} & \mu_1\omega_1 e^{-i\omega T} & \mu_2\omega_2 e^{-i\omega_2 T} & -\mu_2\omega_2 e^{i\omega_2 T} \end{pmatrix} \begin{pmatrix} D_1^+ \\ D_1^- \\ D_2^+ \\ D_2^- \end{pmatrix} = \begin{pmatrix} 0 \\ 0 \\ 0 \\ 0 \end{pmatrix}. \tag{18}$$

The condition that the determinant of the four by four matrix must vanish renders the eigenvalues $\omega(k)$, while these four homogeneous equations determine three of the four D amplitudes in terms of a selected fourth. (In principle, the fourth, undetermined amplitude is associated with the amplitude of the excitation.)

It is convenient to normalize the frequency ω and the wave number k by means of the modulation frequency Ω:

$$\hat{\omega} = \omega/\Omega, \qquad \hat{k} = k/\Omega\sqrt{\bar{\varepsilon}\bar{\mu}}. \tag{19}$$

We also introduce a parameter $\tau = t_1/T$. For $\tau < 0.5$, $t_1 < t_2$. while for $\tau > 0.5$, $t_1 > t_2$. The next section will be limited to the simplest case, $t_1 = t_2$, namely. $\tau = 0.5$. The aforementioned determinantal equation can be solved exactly, to yield—after considerable algebra—the reduced frequency $\hat{\omega}$ as function of the reduced wave number $\hat{k}$:

$$cos(2\pi\hat{\omega}) = \frac{1}{2}(1-M_A)cos\left\{2\pi\hat{k}\left[\frac{\tau}{M^+} - \frac{1}{M^-}(1-\tau)\right]\right\} + \frac{1}{2}(1+M_A)cos\left\{2\pi\hat{k}\left[\frac{\tau}{M^+} + \frac{1}{M^-}(1-\tau)\right]\right\}, \tag{20}$$

$$M^{\pm} = \sqrt{(1 \pm m_\varepsilon)(1 \pm m_\mu)}, \tag{21}$$

$$M_A = (1 - m_\varepsilon m_\mu)/M^- M^+. \tag{22}$$

This transcendental dispersion relation involves three parameters: τ, the dielectric modulation m_ε and the magnetic modulation m_μ. It is periodic in $\hat{\omega}$ with the period 1 (corresponding to the period Ω for ω), however it is not, in general, periodic in $\hat{k}$. This situation, of course, reflects the periodicity in time, rather than space, of our parameters. For $m_\mu = 0$ and $\tau = 1/2$, Eq. (20) reduces to results previously reported in Refs. [11–13].

It is instructive to examine the low-frequency, long-wavelength limit, namely $\hat{\omega} \to 0$ and $\hat{k} \to 0$, in which case Eq. (20) is reduced to

$$\frac{\omega}{k} = \left[\sqrt{\frac{\bar{\varepsilon}(1-m_\varepsilon^2)}{1+m_\varepsilon - 2m_\varepsilon\tau}}\sqrt{\frac{\bar{\mu}(1-m_\mu^2)}{1+m_\mu - 2m_\mu\tau}}\right]^{-1}. \tag{23}$$

As seen, in this limit, the phase velocity is constant and the $\omega(k)$ dispersion is linear. The same limit was investigated in Ref. [8] (supplement D) for purely electric modulation ($m_\mu = 0$ and $\bar{\varepsilon} = 1$) and $\varepsilon(t)$ with an arbitrary profile, with the following result for the effective relative permittivity:

$$1/\tilde{\varepsilon} = \frac{1}{T}\int_0^T [1/\varepsilon(t)]dt. \tag{24}$$

For the profile in Eq. (1) this reduces to

$$\tilde{\varepsilon} = \sqrt{\frac{\bar{\varepsilon}(1-m_\varepsilon^2)}{1+m_\varepsilon - 2m_\varepsilon\tau}}. \tag{25}$$

This is the same as Eq. (24) for $m_\mu = 0$. This suggests that, for purely magnetic modulation ($m_\varepsilon = 0$ and $\bar{\mu} = 1$) the ω/k slope is given by

$$\tilde{\mu} = \sqrt{\frac{\bar{\mu}(1-m_\mu^2)}{1+m_\mu - 2m_\mu\tau}}. \tag{26}$$

Thus, in the general case of modulation, $\omega/k = (\tilde{\varepsilon}\tilde{\mu})^{-1}$.

III. BAND STRUCTURE AND FIELDS FOR $t_1 = t_2$

In the following three sections, we will limit the consideration to the case of equal sections t_1 and t_2, namely, $\tau = 1/2$.

A. Unequal modulations of the permittivity and permeability, $m_\varepsilon \neq m_\mu$

In Fig. 2, we present the PBS corresponding to the modulations $m_\varepsilon = 0.5$ and $m_\mu = -0.1$; the different algebraic signs indicate that $\varepsilon(t)$ and $\mu(t)$ oscillate out of phase in this example. The two frequency periods (corresponding to $0 < \omega < \Omega$ and $\Omega < \omega < 2\Omega$) indicate that the PBS is periodic in the wave frequency, the period being the modulation frequency. The first nine k-bands are labeled as $p = 1, 2, \ldots, 9$ and are separated by k gaps, $\Delta k_{p,p+1} = k_{p+1} - k_p$, that are delimited by the k values at its two sides taken for $\omega = (1/2)n\Omega$ with an arbitrary integer n. The inset in the figure zooms in at the low-frequency, long-wavelength limit. As can be expected, the slope of the straight line is indeed given by (23).

It is interesting to compare Fig. 2—for square modulation—with PBSs for harmonic modulation. Examples of the latter are given by Fig. 3 of Ref. [8] for $m_\mu = 0$ and Fig. 1 of Ref. [14] for $m_\varepsilon \neq m_\mu$. There is a qualitative difference, namely, for harmonic modulation there are no band gaps between the bands $p = 2$ and $p = 3$, $p = 4$ and $p = 5$, etc, while, for the square modulation, finite gaps $\Delta k_{2,3}$, $\Delta k_{4,5}$, etc. appear in Fig. 2. We also note a quantitative

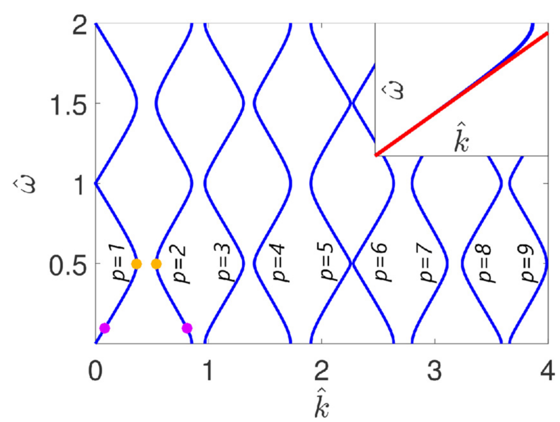

FIG. 2. Photonic band structure (PBS) for the reduced frequency $\hat{\omega}$ versus reduced wave number $\hat{k}$, as defined in Eq. (19). Here $t_1 = t_2(\tau = 0.5)$ and the electric and magnetic modulations are out of phase, $m_\varepsilon = 0.5$ and $m_\mu = -0.1$. Two periods of the frequency (period $\Omega = 2\pi/T$) are presented and the first nine k bands are labeled by the index p. The PBS is depicted in blue lines for real ω. The inset zooms in on the low-frequency, long-wavelength behavior, comparing with the limiting value of the phase velocity (23).

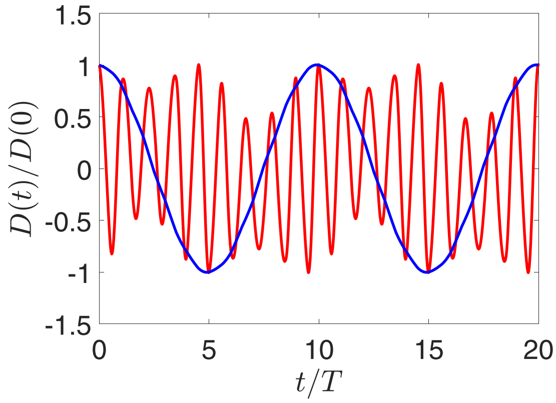

FIG. 3. Normalized displacement fields for the first two bands ($p = 1$ in blue line and $p = 2$ in red line) in Fig. 2, calculated at $\omega = 0.1\Omega$, namely at two pink dots there.

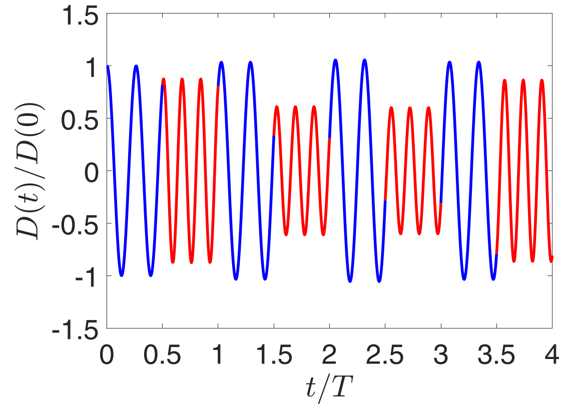

FIG. 4. As in Fig. 3 for the band $p = 15$. Because of the large k value of this band, the periods $T_1 = 2\pi/\omega_1 = 0.179T$ (blue line) and $T_2 = 2\pi/\omega_2 = 0.1147T$ (red line) are clearly discernible within each period T; see Eq. (9).

difference: while, for the harmonic modulation, only the first gap $\Delta k_{1,2}$ is appreciable, there are sizable gaps between all the bands for the square modulation in Fig. 2. And, these gaps do not diminish gradually as p increases; $\Delta k_{p,p+1}$ has a complicated dependence on the modulations. For example, in Fig. 2, $\Delta k_{5,6}$ is the smallest gap, although it is flanked by the two largest gaps, $\Delta k_{4,5}$ and $\Delta k_{6,7}$. This behavior is apparently related to the presence of high harmonics in the square profile of Fig. 1.

Turning to the eigenvector problem of Eq. (18), the $D_{1,2}$ coefficients depend on the values of ω and k and, therefore, for a given ω must be determined separately for each band p. (Only for a well defined system, excited by a source, is it possible to determine the relative contributions to the fields for each band p.) We will evaluate the fields at the point $x = 0$, so, according to Eq. (6), $D(x, t) = D(t)$. In Appendix, we prove that the fields corresponding to the eigenvalues of Eq. (18) are stable. A complete interpretation of the behavior of $D(t)$ can involve oscillations with four frequencies: the modulation frequency Ω, the Bloch-Floquet frequency ω, and the auxiliary frequencies ω_1 and ω_2 given in Eq. (9). The gross behavior can be understood by the following formulation of the Bloch-Floquet theorem [from which Eq. (10) can be easily derived]: $D(t)$ must be the product of $e^{-i\omega t}$ and a function that has the periodicity of the modulation $2\pi/\Omega$. For $\omega < \Omega$ (as is the situation in the examples below), this means that relatively rapid oscillations of frequency Ω are modulated by a relatively slowly oscillating envelope of frequency ω. This is clearly observed in Fig. 3 for the second band ($p = 2$) in Fig. 2, displaying the periods T and $10T$ (corresponding to our selection $\omega = 0.1\Omega$). On the other hand, $D(t)$ for the first band ($p = 1$) has the form $\cos(\omega t)$ with $\omega = 0.1\Omega$, as would be appropriate for a medium with constant permittivity and permeability. This is hardly surprising, this mode is in the low-frequency, long wavelength region, with phase velocity given by Eq. (23).

Why is there no trace of oscillations with the frequencies ω_1 and ω_2 in Fig. 3? That's because the corresponding periods, $T_1 = 2\pi/\omega_1 = 13.51T$ and $T_2 = 2\pi/\omega_2 = 8.62T$ are too large to visibly affect the behavior within a single period T. We can expect ω_1 and ω_2 to make a difference if they are sufficiently large to have T_1 and T_2 smaller than T. Eq. (9) suggests that this could be achieved for large values of k, namely for distant bands ($p \gg 1$). With this motivation, in Fig. 4, we plot $D(t)$ for the band $p = 15$; now $T_1 = 0.179T$ and $T_2 = 0.1147T$. And now, indeed, we can observe oscillations of period T_1 (T_2) in the first (second) half of each period T.

The case $\omega = (1/2)\Omega$ (orange points in Fig. 2) merits special attention. We find numerically that in Eq. (8) $D_1^- = D_1^{+*}$ and $D_2^- = D_2^{+*}$, the asterisk meaning "complex conjugate." This implies that $D(t)$ is proportional to $\cos[(1/2)\Omega t + \phi_{1,2}]$, where $\phi_{1,2}$ are phase angles corresponding to $k_{1,2}(\omega = \Omega/2)$. It then follows from Eq. (6) that $\mathrm{Re}(D(x, t))$ is proportional to $\cos(k_{1,2}x)\cos[(1/2)\Omega t + \phi_{1,2}]$, hence describing stationary waves for the first two bands. This is hardly surprising in view of recent results for harmonic modulation [58] and explains the behavior of both bands in Fig. 5 as given by a simple oscillation of frequency $(1/2)\Omega$, rather than the propagating Bloch-Floquet wave form of Fig. 3 for $p = 2$.

The continuity of $D(t)$, explicitly stated in Eq. (11), is manifest in Figs. 3–5. On the other hand, because $\varepsilon(t)$ is discontinuous at the times $t_d = (T/2)n$ (n being an arbitrary

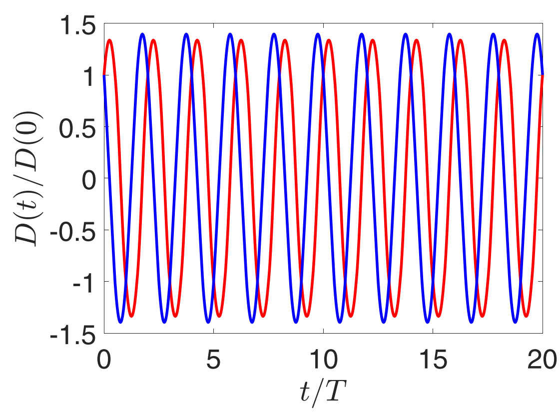

FIG. 5. Normalized displacement fields for the first two bands ($p = 1, 2$) in Fig. 2 for the frequency $\omega = 0.5\Omega$ (at the orange dots in Fig. 2).

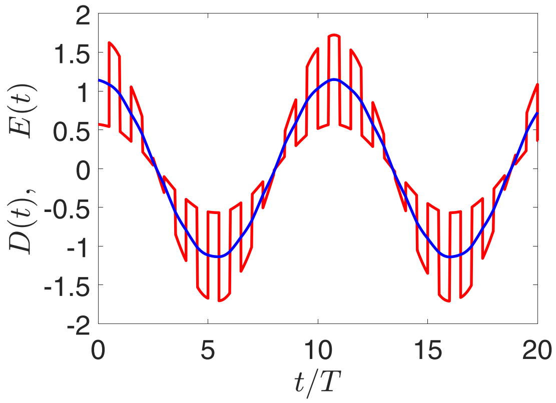

FIG. 6. The displacement field $D(t)$ (blue line) and the electric field $E(t)$ (red line) for the first band in Fig. 2 at $\omega = 0.1\Omega$. While $D(t)$, according to Eq. (11), is continuous across the discontinuities of $\varepsilon(t)$ and $\mu(t)$ at all the integer multiples of $(1/2)T$, $E(t) = D(t)/\varepsilon(t)$ is obviously discontinuous.

integer), we can expect to find corresponding discontinuities in the electric field $E(t)$. This is confirmed by Fig. 6, that compares the $E(t)$ and $D(t)$ fields.

B. Equal, out-of-phase modulations of $\varepsilon(t)$ and $\mu(t)$

In this subsection we deal with electric and magnetic modulations of equal magnitude that are, however, out of phase. This situation can be described by means of a single modulation parameter $m = m_\varepsilon = -m_\mu$. Equation (20) then greatly simplifies:

$$\cos\left(\frac{2\pi\hat{k}}{\sqrt{1-m^2}}\right) = m^2 + (1-m^2)\cos(2\pi\hat{\omega}). \tag{27}$$

This PBS is periodic in $\hat{k}$, as see in Fig. 7.

The solutions for the odd and even k bands at their waists ($\omega = \Omega/2$) can be written as follows:

$$\hat{k}_p = \frac{\sqrt{1-m^2}}{2}\left(p - 1 + \frac{|\cos^{-1}(2m^2-1)|}{\pi}\right),$$

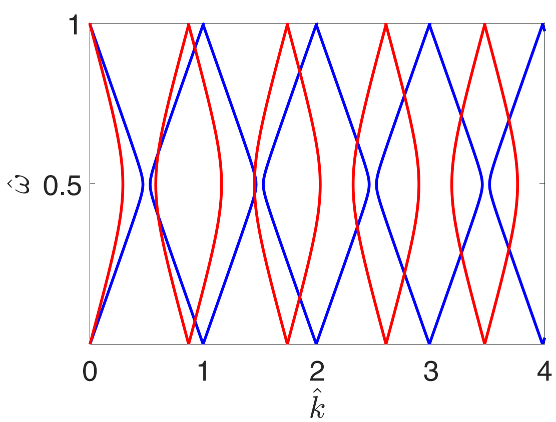

FIG. 7. PBS for out-of-phase modulations of equal magnitudes: $m_\varepsilon = -m_\mu = m = 0.1$ (blue line) and 0.5 (red line). The band gaps are all equal for a given m, as given by Eq. (30).

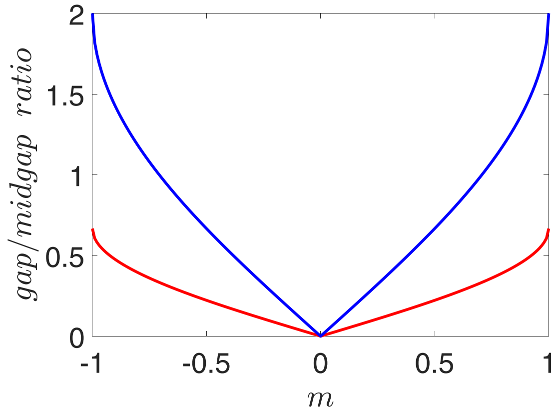

FIG. 8. Gap/midgap ratios between the bands 1 and 2 (blue line) and 3 and 4 (red line) in Fig. 7, as function of the modulation m, according to Eq. (32).

$$p = 1, 3, 5\ldots, \tag{28}$$

$$\hat{k}_{p+1} = \frac{\sqrt{1-m^2}}{2}\left(p + 1 - \frac{|\cos^{-1}(2m^2-1)|}{\pi}\right),$$

$$p = 1, 3, 5\ldots \tag{29}$$

with the understanding that $0 < |\cos^{-1}(2m^2-1)| < \pi$. The separation between two adjacent bands is then

$$\Delta\hat{k}_{p,p+1} = \sqrt{1-m^2}\left(1 - \frac{|\cos^{-1}(2m^2-1)|}{\pi}\right) \tag{30}$$

independently of the band index p. It also follows that the midgap point is

$$\hat{k}_{p,p+1} = \frac{\hat{k}_p + \hat{k}_{p+1}}{2} = p\frac{\sqrt{1-m^2}}{2} \tag{31}$$

and, therefore, the gap-midgap ratio is

$$\frac{\Delta\hat{k}_{p,p+1}}{\hat{k}_{p,p+1}} = \frac{2}{p}\left(1 - \frac{|\cos^{-1}(2m^2-1)|}{\pi}\right). \tag{32}$$

Unlike the behavior we've seen in Fig. 2, Eq. (30) indicates that the band gaps $\Delta\hat{k}_{p,p+1}$ are all the same, as confirmed by Fig. 7 for two values of the modulation m. It is noteworthy that here there are no gaps between the bands 2 and 3, 4 and 5, etc (as found in the general case of modulation, Fig. 2). The gap-midgap ratio, Eq. (32) is plotted in Fig. 8 for the first and second gaps.

C. Equal, in-phase modulations of $\varepsilon(t)$ and $\mu(t)$

In this subsection the electric and magnetic modulations are assumed to be equal in sign, as well as in magnitude, namely, $m_\varepsilon = m_\mu = m$. This is to say that the maximum (and also the minimum) values of $\varepsilon(t)$ and of $\mu(t)$ occur simultaneously in the same time intervals. Eq. (20) greatly simplifies, resulting in

$$\hat{k}_p = (1-m^2)\left\{(-1)^{p-1}\hat{\omega} + \left[\frac{p}{2} - \frac{1+(-1)^{p-1}}{4}\right]\right\} \tag{33}$$

with p being the band number. The PBS, displayed in Fig. 9 for two values of the modulation, is a collection of straight

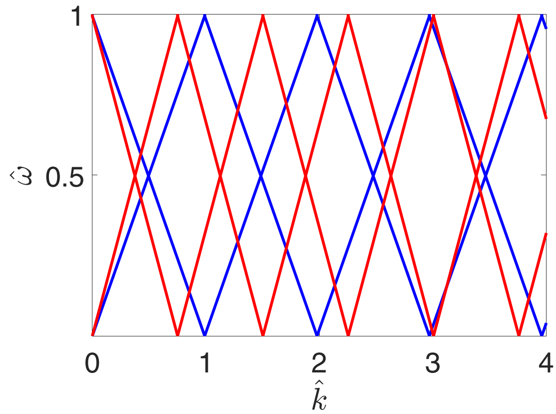

FIG. 9. The PBS for equal (in-phase) modulations are distinguished by constant (positive and negative) group velocities and by the absence of band gaps. Two cases of modulation are considered: $m = 0.1$ (blue lines) and $m = 0.5$ (red lines). The slopes are given by Eq. (33).

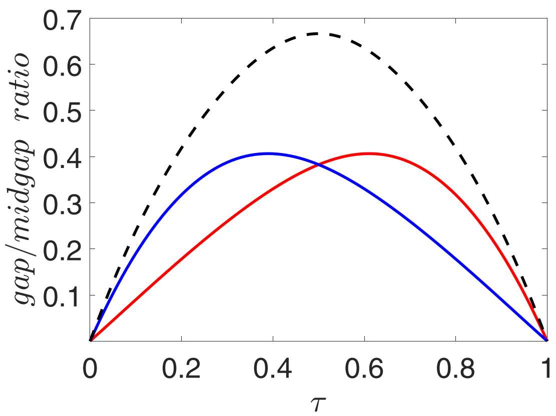

FIG. 10. First gap/midgap ratio as function of the fraction $\tau = t_1/T$ (see Fig. 1) for three cases of out-of-phase modulations: $m_\varepsilon = -0.5$ and $m_\mu = 0.1$ (blue line), $m_\varepsilon = 0.5$ and $m_\mu = -0.1$ (red line), and $m_\varepsilon = 0.5$ and $m_\mu = -0.5$ (black line).

lines with positive and negative slopes that increase with m, diverging for $m \to 1$. Not surprisingly, this is the same slope as obtained in Eq. (23) in the $\omega \to 0$, $k \to 0$ limit in the special case that $\tau = 0.5$ and $m_\varepsilon = m_\mu = m$. The most notable aspect of Fig. 9 is the total absence of band gaps, as was also found previously for harmonic modulations of $\varepsilon(t)$ and $\mu(t)$ [14]. In order to explain this, we now explore the eigenvectors.

It turns out that, for $\omega/k > 0$, $D^-_{1,2} = 0$, while, for $\omega/k < 0$, we get $D^+_{1,2} = 0$. This means that for the positive (negative) slope there exist only waves that propagate to the right (left). In other words, no reflections arise at the temporal discontinuities t_d. This can be explained by means of the characteristic impedances. For, it follows from Eqs. (1) and (2) that μ_1/ε_1 and μ_2/ε_2 are both equal to $\bar{\mu}/\bar{\varepsilon}$ for $m_\varepsilon = m_\mu$. The characteristic wave impedances Z in the time intervals $t_1(= T/2)$ and $t_2(= T/2)$ are then equal:

$$Z_1 = \sqrt{\frac{\mu_1}{\varepsilon_1}} = \sqrt{\frac{\bar{\mu}}{\bar{\varepsilon}}} = \sqrt{\frac{\mu_2}{\varepsilon_2}} = Z_2. \tag{34}$$

The average impedance $\bar{Z} = \sqrt{\bar{\mu}/\bar{\varepsilon}}$ has been defined in terms of the average permittivity $\bar{\varepsilon}$ and the average permeability $\bar{\mu}$ (see Fig. 1). This allows us to associate the k-gaps with reflections of the fields at temporal interfaces that involve discontinuities of the characteristic wave impedance.

IV. UNEQUAL TIME INTERVALS t_1 AND t_2

Figure 1 shows an example of two steps of unequal lengths $t_1 \neq t_2$ that make up a modulation period $(t_1 + t_2 = T)$. In terms of the parameter $\tau = t_1/T$, this can be expressed as $\tau \neq 0.5$. However, the former Sec. III was restricted to the simplest situation, $t_1 = t_2$ or $\tau = 0.5$. In the present section, we briefly explore how the parameter τ affects the first band gap.

Figure 10 presents the gap/midgap ratio, as function of τ, for three cases of out-of-phase modulations (different signs of m_ε and m_μ). For $m_\varepsilon = 0.5$ and $m_\mu = -0.5$ (black line), the largest ratio is obtained for $\tau = 0.5$, decreasing symmetrically as τ approaches the limiting values 0 and 1, at which the ratio vanishes because $\varepsilon(t)$ and $\mu(t)$ become constant in these limits. For $\tau = 0.5$, the PBS is shown in Fig. 7 (blue line), so the constant gaps $\Delta\hat{k}$ there, given by Eq. (30), are the largest that can be attained for $m_\mu = -m_\varepsilon$. On the other hand, for $|m_\varepsilon| \neq |m_\mu|$ (blue and red lines), the gap/midgap ratios are asymmetric with respect to τ, peaking at $\tau = 0.6104$ for $m_\varepsilon = 0.5$ and $m_\mu = -0.1$ and at $\tau = 0.3896$ for $m_\varepsilon = -0.5$ and $m_\mu = 0.1$. These two values of τ are complementary in the sense that they sum up to 1.

It is also possible to prove that, for given values of m_ε and m_μ the maximum gap/midgap ratio is obtained for the following value of τ:

$$\tau = \frac{1}{1 + \sqrt{\frac{(1-m_\varepsilon)(1-m_\mu)}{(1+m_\varepsilon)(1+m_\mu)}}}. \tag{35}$$

V. OPTICAL RESPONSE

Up to this point we considered propagation in a boundless modulated medium; in this section we deal with the optical response of a dielectric slab whose permittivity and permeability are modulated periodically in time. The slab extends from $x = -L/2$ to $L/2$ and is bounded on both sides by media of (static) permittivity ε_1 and permeability μ_1. We wish to calculate the reflected and transmitted response to a normally incident plane harmonic wave of circular frequency ω and wave vector $k_0 = \omega\sqrt{\varepsilon_1\mu_1}$; its electric and magnetic fields are defined as

$$E_{\text{inc}}(x, t) = E_0 e^{ik_0(x+L/2)} e^{-i\omega t}, \tag{36}$$

$$H_{\text{inc}}(x, t) = \sqrt{\frac{\varepsilon_1}{\mu_1}} E_0 e^{ik_0(x+L/2)} e^{-i\omega t}. \tag{37}$$

Our dispersion relation Eq. (20) predicts that inside the dynamic slab the wave fields will be superpositions of plane waves with wave vectors $k_p(\omega)$, $p = 1, 2, \ldots$ Moreover, for a given ω all the harmonics $\omega - n\Omega$, $n = \pm 1, \pm 2, \ldots$ can be excited. Therefore we express the electric field as follows:

$$E_{\text{slab}}(x, t) = \sum_n \sum_{p=1} e_{pn} e^{-i(\omega - n\Omega)t} [A_p e^{ik_p(x+L/2)} + B_p e^{-ik_p(x+L/2)}] \tag{38}$$

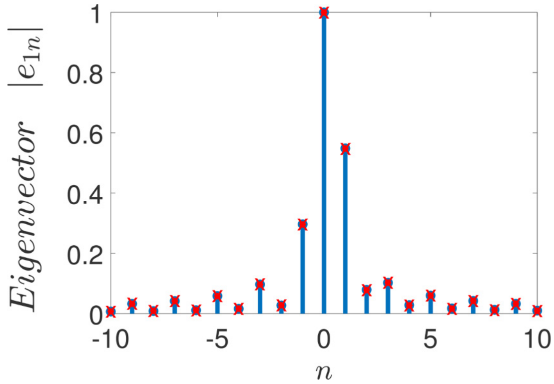

FIG. 11. Electric field amplitudes $|e_{1n}|$ for the first k-band ($p = 1$) and harmonics n from -10 to $+10$. The reduced frequency is $\hat{\omega} = 0.4$ and the modulations are $m_\varepsilon = 0.5$, $m_\mu = -0.1$. These eigenvectors were calculated by two methods: the Fourier representation of Krönig-Penney approach, Eq. (18) (blue lines), and the eigenvalue equation Eq. (39) for the bulk problem (red dots).

Here, A_p and B_p are the amplitudes, respectively, of the partial waves that propagate to the right and left. The eigenvectors of the electric field e_{pn} are obtained from the eigenvalue problem for the boundless (bulk) medium, as in [14]:

$$\sum_{m,n}[\hat{\mu}_{l-m}\hat{\varepsilon}_{m-n}(\hat{\omega}-l)(\hat{\omega}-m)-\hat{k}_p^2\delta_{ln}\delta_{m0}]e_{pn}(\hat{\omega})=0$$
$$l,m,n=0,\pm1,\pm2,\dots \tag{39}$$

Here, the normalized Fourier coefficients $\hat{\mu}_n$ and $\hat{\varepsilon}_n$ must be calculated, of course, for the square profiles of $\mu(t)$ and $\varepsilon(t)$ in Fig. 1.

The magnetic field $H_{\text{slab}}(x,t)$ has the very same form as $E_{\text{slab}}(x,t)$, Eq. (38), but with the e_{pn} replaced by the corresponding eigenvectors h_{pn}. These can be also obtained from the Ampére-Maxwell law as

$$h_{pn}=\sum_m\sqrt{\frac{\bar{\varepsilon}}{\bar{\mu}}}\frac{\hat{\varepsilon}_{n-m}(\hat{\omega}-n)}{\hat{k}_p}e_{pm} \tag{40}$$

The reduced wave vectors $\hat{k}_p(\hat{\omega})$ in Eqs. (39) and (40) are most conveniently obtained from (20). As for the eigenvectors $e_{pn}(\hat{\omega})$, while they can be calculated by the KP approach from (18), we find it more expedient to employ Eq. (39). The results are practically the same provided that the matrix used in Eq. (39) is large enough. To illustrate this, we apply both methods to calculate the eigenvectors $e_{1n}(\hat{\omega}=0.4)$ for the first band ($p=1$) and 21 different harmonics n. The excellent coincidence displayed by the frequency comb in Fig. 11 confirms the equivalence of the two methods.

The electric and magnetic fields that are reflected by the slab and the transmitted electric and magnetic fields are given by the following four equations:

$$E_r(x,t)=\sum_n E_n^r e^{-ik_n^r(x+L/2)}e^{-i(\omega-n\Omega)t}, \tag{41}$$

$$H_n^r(x,t)=-\sqrt{\frac{\varepsilon_1}{\mu_1}}E_r(x,t), \tag{42}$$

$$E_t(x,t)=\sum_n E_n^t e^{\,ik_n^t(x-L/2)}e^{-i(\omega-n\Omega)t}, \tag{43}$$

$$H_t(x,t)=\sqrt{\frac{\varepsilon_1}{\mu_1}}E_t(x,t). \tag{44}$$

The E and H fields must be both continuous at the slab boundaries $x=\pm L/2$ at every instant of time t. The corresponding four equations are gotten by using Eqs. (36) and (37) for the incident fields, Eqs. (41)–(44) for the reflected and transmitted fields, and Eqs. (38)–(40) for the fields inside the slab:

$$\frac{E_n^r}{E_0}=r_n=\sum_{p=1}\left(\frac{A_p}{E_0}+\frac{B_p}{E_0}\right)e_{pn}-\delta_{n0}, \tag{45}$$

$$\frac{E_n^t}{E_0}=t_n=\sum_{p=1}\left(\frac{A_p}{E_0}e^{i\hat{k}_p\nu}+\frac{B_p}{E_0}e^{-i\hat{k}_p\nu}\right)e_{pn}, \tag{46}$$

$$2\delta_{n0}=\sum_{p=1}\left[e_{pn}+\sum_m\frac{\hat{\varepsilon}_{n-m}(\hat{\omega}-n)\hat{Z}}{\hat{k}_p}e_{pm}\right]\frac{A_p}{E_0}$$
$$+\sum_{p=1}\left[e_{pn}-\sum_m\frac{\hat{\varepsilon}_{n-m}(\hat{\omega}-n)\hat{Z}}{\hat{k}_p}e_{pm}\right]\frac{B_p}{E_0}, \tag{47}$$

$$0=\sum_{p=1}\left[e_{pn}-\sum_m\frac{\hat{\varepsilon}_{n-m}(\hat{\omega}-n)\hat{Z}}{\hat{k}_p}e_{pm}\right]e^{i\hat{k}_p\nu}\frac{A_p}{E_0}$$
$$+\sum_{p=1}\left[e_{pn}+\sum_m\frac{\hat{\varepsilon}_{n-m}(\hat{\omega}-n)\hat{Z}}{\hat{k}_p}e_{pm}\right]e^{-i\hat{k}_p\nu}\frac{B_p}{E_0}. \tag{48}$$

In these equations, $\hat{Z}$ is the average impedance of the slab $\sqrt{\bar{\mu}/\bar{\varepsilon}}$ normalized by the impedance $\sqrt{\mu_1/\varepsilon_1}$ of the bounding medium, namely, the relative impedance,

$$\hat{Z}=\sqrt{\frac{\varepsilon_1}{\mu_1}}\sqrt{\frac{\bar{\mu}}{\bar{\varepsilon}}}. \tag{49}$$

We have also normalized the slab thickness L by defining the parameter [22]

$$\nu=\Omega\sqrt{\bar{\varepsilon}\bar{\mu}}L. \tag{50}$$

Equations (47) and (48) permit us to calculate the relative electric field amplitudes A_p/E_0 and B_p/E_0. Once determined, the reflection coefficients r_n and transmission coefficients t_n can be found from the Eqs. (45) and (46), respectively. All these fields display the characteristic discreteness $|\omega-n\Omega|$ (or, in normalized form, $|\hat{\omega}-n|$) of the frequency comb.

In what follows, we show examples of partial reflection and transmission spectra, $|r_n(\hat{\omega})|^2$ and $|t_n(\hat{\omega})|^2$, for three different cases of the modulations m_ε and m_μ. In all of these, we chose the thickness parameter ν to have the value 1, well removed from special values that give rise to parametric resonances [20,21]. Such resonances for square modulations of the permittivity and permeability will be investigated in future work.

In Figs. 12(a) and 12(b), we display the reflectance and transmittance spectra $|r_n(\hat{\omega})|^2$ and $|t_n(\hat{\omega})|^2$ for $m_\varepsilon = 0.5$ and $m_\mu=-0.1$, namely, different and out-of-phase electric and magnetic modulations. Summing over all the harmonics n, in Fig. 12(c), we obtain the total reflectance $R(\hat{\omega})=|r_0(\hat{\omega})|^2+|r_1(\hat{\omega})|^2+\dots$ and transmittance $T(\hat{\omega})=|t_0(\hat{\omega})|^2+|t_1(\hat{\omega})|^2+\dots$ While the oscillatory behavior reminds of Fabry-Perot oscillations, here we have

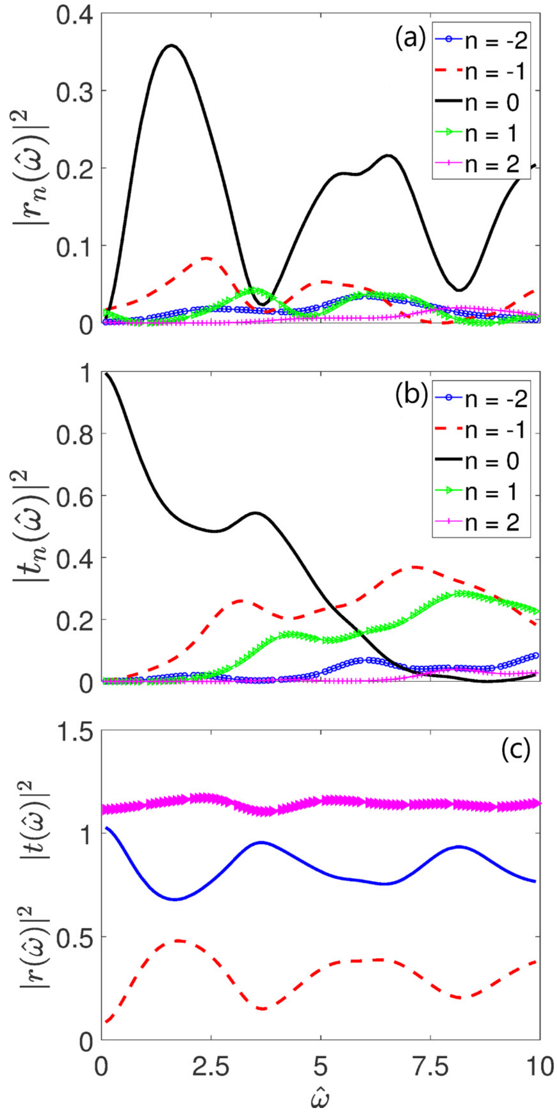

FIG. 12. (a)Reflectance and (b)transmittance for the harmonics $n = 0, \pm 1$, and ± 2 assuming a relative impedance $\hat{Z} = 0.5$ and modulations $m_\varepsilon = 0.5$ and $m_\mu = -0.1$. The total reflectance $R(\hat{\omega})$ (red line), total transmittance $T(\hat{\omega})$ (blue line), and $R(\hat{\omega}) + T(\hat{\omega})$ (pink line), obtained by summing over all the harmonics n, is shown in (c).

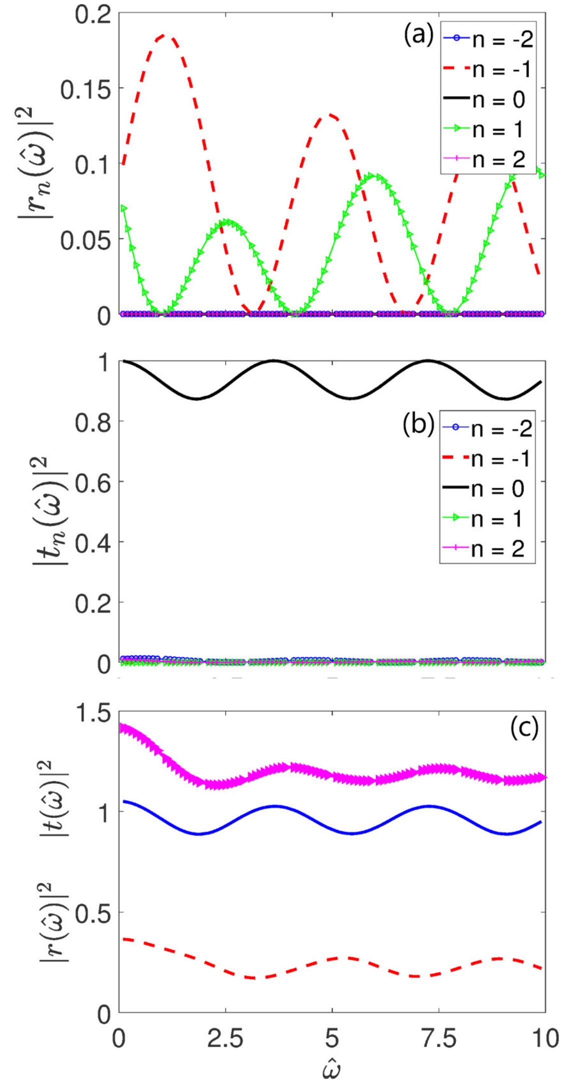

FIG. 13. As in Fig. 12 for equal and out-of-phase modulations $m_\varepsilon = 0.5$ and $m_\mu = -0.5$, with $\hat{Z} = 1$ and $\nu = 1$.

interference of multiple waves with wavelengths $\lambda_p(= 2\pi/k_p,\ p = 1, 2, \dots)$. These obey a complex, nonlinear band structure with k-gaps, see Fig. 2. It is for this reason that the oscillations are not harmonic and that $|r_n(\hat{\omega})|$ and $|t_n(\hat{\omega})|$ never reach the values 0 or 1. Moreover, we find that $R(\hat{\omega}) + T(\hat{\omega}) > 1$, implying energy transfer from the source of modulation to the slab [22,23].

The case of equal, however out-of-phase modulations, $m_\varepsilon = 0.5$ and $m_\mu = -0.5$, is taken up in Fig. 13, displaying the reflectances and transmittances for the same five harmonics n as in Fig. 12, however with $\hat{Z} = 1$ for the relative impedance. Interestingly, only the harmonics $n = \pm 1$ are prominent in the reflectance, while only the fundamental harmonic $n = 0$ is appreciable in the transmittance. This signifies that, for equal out-of-phase modulations, the transmitted light is not given by a frequency comb, but rather, is essentially monochromatic, just as the incident light. However, the amplitude of the transmitted energy is an oscillatory function of the frequency. Further, $|r_{\pm 1}(\hat{\omega})|$ can vanish for certain values of $\hat{\omega}$ and $|t_0(\hat{\omega})|$ can reach the value 1 for some $\hat{\omega}$. It is seen again that $R(\hat{\omega}) + T(\hat{\omega}) > 1$ for all $\hat{\omega}$.

Figure 14 shows the optical response of a slab with equal in-phase modulations $m_\varepsilon = m_\mu = 0.5$ and relative impedance $\hat{Z} = 1$. In this very special case, according to Eq. (34), the impedance remains unchanged at each abrupt temporal transition of the permittivity and permeability. Moreover, there are also no impedance changes at the boundary surfaces of the slab; that's because we made the choice $\hat{Z} = 1$ for the relative impedance in Eq. (49). These conditions ensure that no light is reflected at either the temporal or the spacial interfaces, namely, $r_n = 0$ for all the harmonics.

As a consequence, no light is reflected by the slab for any frequency, $r_n = 0,\ n = 0, 1, \dots$ On the other hand, the transmitted field displays oscillations for all the harmonics, as seen in Fig. 14(a). Curiously, adding up the contributions from

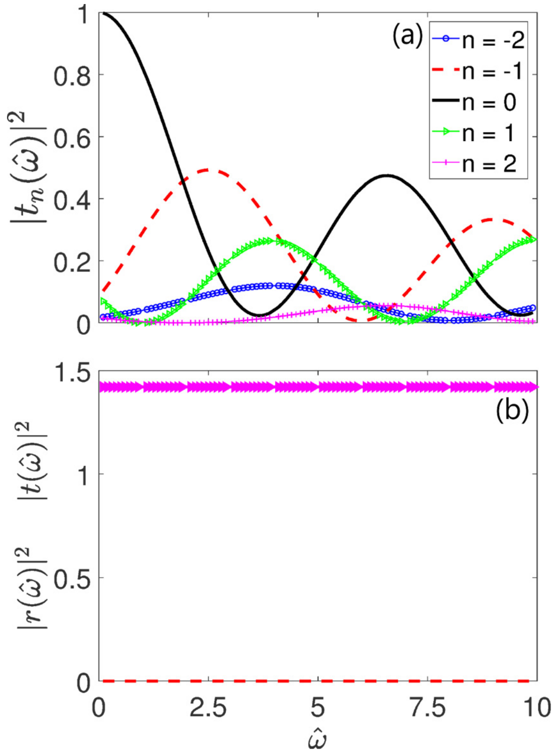

FIG. 14. (a)Transmittance for five harmonics n, assuming $\nu = 1$, $\hat{Z} = 1$, and $m_\varepsilon = m_\mu = 0.5$. (b)Total reflectance (dashed line) and transmittance (blue line) by the slab.

all the harmonics, the total transmittance $T(\hat{\omega})$ is constant (independent of frequency) at the value 1.4, approximately. This corresponds to a huge transfer of energy from the source of modulation to the transmitted light.

To complete this study of the optical response, we also investigated the behavior of the fields inside the plate. Again we consider equal, in-phase modulations, $m_\varepsilon = m_\mu = 0.5$ and parameter values $\nu = 1, \hat{Z} = 1$, and $\hat{\omega} = 1/2$. The normalized electric field amplitudes of the same five harmonics n as in Fig. 14 are shown in Fig. 15 as function of the position x in the slab. At the left side interface ($x = -L/2$), the amplitudes of all the harmonics vanish, with the exception of the fundamental $n = 0$, this amplitude coinciding with that of the incident field. This confirms the fact that no light is reflected for $\hat{Z} = 1$ and equal, in-phase modulations, as we have observed in Fig. 14(b), dashed line. As x increases, so do the amplitudes of all the harmonics $n \neq 0$, reaching maximum values at the right-side interface of the slab. As also in Fig. 14(a), at $x = L/2$, the largest (second largest) amplitude is obtained for the harmonic $n = 0$ ($n = -1$).

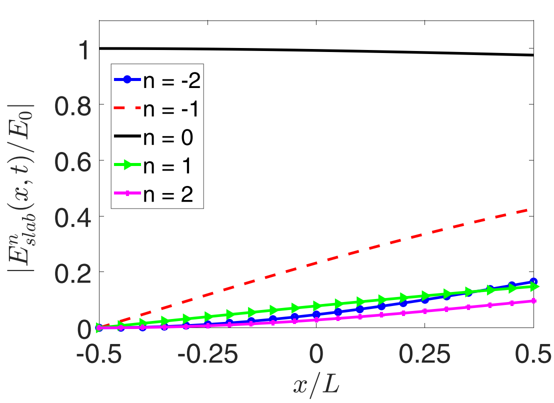

FIG. 15. Electric field amplitudes, as function of the position x in the slab, for five harmonics n, normalized by the amplitude of the incident field. Parameters as in Fig. 14 and $\hat{\omega} = 0.5$.

VI. CONCLUSION

We have presented a comprehensive study of the photonic band structure and optical response of a temporal photonic crystal with square modulations in time of its permittivity and permeability (Fig. 1). Because the abrupt discontinuities of $\varepsilon(t)$ and $\mu(t)$ allow us to take advantage of the continuity of the $D(t)$ and $B(t)$ fields, this problem is amanable to the Krönig-Penney method of Solid State physics, leading to an analytic formula for the band structure $k(\omega)$ Eq. (20). This PBS is periodic in the frequency ω, the period being the modulation frequency Ω. An infinite number of k bands, separated by k gaps, is obtained; these gaps are typically much larger than those found for harmonic modulation [8,14], even for remote bands (with large k values), see Fig. 2. The PBS strongly depends on the modulations m_ε and m_μ of the permittivity and permeability and on the parameter τ [$= t_1/(t_1 + t_2)$], see Fig. 11. For $\tau = 1/2$ and equal out-of-phase modulations ($m_\mu = -m_\varepsilon$), the PBS is periodic in k and all the prohibited bands have the same width Δk, see Fig. 7. If, on the other hand, the modulations are in phase ($m_\mu = m_\varepsilon$) the PBS degenerates into a system of intersecting straight lines with no band gaps, see Fig. 9. This is a result of the continuity of the impedance $\sqrt{\mu/\varepsilon}$ across the temporal interfaces, thus obviating reflections. It suggests that, in general, k-gaps arise because temporal diffraction at discontinuities of the impedance.

We have also calculated the eigenfunctions $D(t)$ of the displacement field. As required by the Bloch-Floquet theorem, they have the form of a periodic function with period Ω, modulated by $e^{-i\omega t}$, see Figs. 3–6. In the special case that $\omega = (1/2)\Omega$, or $(3/2)\Omega$, etc., they are standing waves, see Fig. 5.

The optical response of a slab to a normally incident plane monochromatic wave is polychromatic; namely, the reflected and transmitted light are composed of "frequency combs" of frequencies $|\omega - n\Omega|, n = \cdots - 1, 0, 1, \ldots$ We have calculated the spectra of reflectances $|r_n(\omega)|^2$ and transmittances $|t_n(\omega)|^2$, see Figs. 12–14, for five harmonics n and also the electric field profile in the slab, Fig. 15. Interesting to note that for equal, however out-of-phase modulations $m_\mu = -m_\varepsilon$ only the fundamental $n = 0$ is prominent in the transmission spectrum. On the other hand, for equal, in-phase modulations $m_\mu = m_\varepsilon$ and unit relative impedance no light is reflected at all by the slab.

APPENDIX: PROOF OF STABILITY

The stability of a temporal photonic crystal can be established using the transition matrix method [43]. According to the stability condition, the eigenvalues λ of the transition matrix must obey the condition $|\lambda| < 1$. To create the transition matrix $\phi(T,0)$ over the period T it is necessary to re-write the Eq. (7) like a state equation where the displacement field $D(t)$ and magnetic field $B(t)$ are elements of the state vector. Due to the square profiles of $\varepsilon(t)$ and $\mu(t)$, Fig. 1, Eq. (7) can be split in two and, for this reason, the state vector is the matrix equation $[D(t), B(t)]^T = W_{1,2}\,[D^+_{1,2}, D^-_{1,2}]^T$. Here, the matrix W_h, Eq. (A1), contains the two linearly independent solutions to the field $D(t)$ according to the Eq. (8) and the magnetic field $B(t)$ calculated from Eq. (4).

$$W_{1,2} = \begin{pmatrix} e^{-i\omega_{1,2}t} & e^{i\omega_{1,2}t} \\ -\frac{\mu_{1,2}\omega_{1,2}}{k}e^{-i\omega_{1,2}t} & \frac{\mu_{1,2}\omega_{1,2}1}{k}e^{i\omega_{1,2}t} \end{pmatrix}. \tag{A1}$$

The $D^+_{1,2}$ and $D^-_{1,2}$ are unknowns used to create a transition matrix $\phi(t_\beta, t_\alpha)$. The transition matrix (A2) relates the fields $[D(t_\beta), B(t_\beta)]$ at the time t_β to the fields $[D(t_\alpha), B(t_\alpha)]$ at the time t_α as initial value:

$$\phi(t_\beta, t_\alpha) = W_{1,2}(t_\beta)W_{1,2}(t_\alpha)^{-1}. \tag{A2}$$

The transition matrix over the period T is the product of the two transition matrices $\phi(T, t_1^+)$ and $\phi(t_1^-, 0)$:

$$\begin{aligned}\phi(T,0) &= \phi(T, t_1^+)\phi(t_1^-, 0)\\ &= W_2(T)W_2(t_1^+)^{-1}W_1(t_1^-)W_1(0)^{-1}.\end{aligned} \tag{A3}$$

The stability condition Eq.(A4) is found when the characteristic polynomial of Eq. (A3) is resolved:

$$|\phi_{11}(T,0) + \phi_{22}(T,0)| \leqslant 2. \tag{A4}$$

After lengthy algebra, the following stability condition is found:

$$\left|\frac{1}{2}(1-M_A)\cos\left\{2\pi\hat{k}\left[\frac{\tau}{M^+} - \frac{1}{M^-}(1-\tau)\right]\right\} + \frac{1}{2}(1+M_A)\cos\left\{2\pi\hat{k}\left[\frac{\tau}{M^+} + \frac{1}{M^-}(1-\tau)\right]\right\}\right| \leqslant 1. \tag{A5}$$

Comparison of Eq.(A5) and the dispersion relation Eq. (18) confirms that the fields $D(t)$ and $B(t)$ are stable when the angular frequency is real and the wave number k correspond to any k band.

[1] F. R. Morgenthaler, Velocity modulation of electromagnetic waves, IRE Trans. Microw. Theory Tech. **6**, 167 (1958).

[2] T. M. Ruiz, C. L. Wright, and J. Smith, Characteristics of electromagnetic waves propagating in time varying media, IEEE Trans. Antenna Propag. **26**, 358 (1978).

[3] C. Caloz and Z.-L. Deck-Léger, Spacetime metamaterials part I: General concepts, IEEE Trans. Antenna Propag. **68**, 1569 (2020).

[4] Y. Xiao, D. N. Maywar, and G. P. Agrawal, Reflection and transmission of electromagnetic waves at a temporal boundary, Opt. Lett. **39**, 574 (2014).

[5] M. Chegnizadeh, K. Mehrany, and M. Memarian, General solution to wave propagation in media undergoing arbitrary transient or periodic temporal variation of permittivity, J. Opt. Soc. Am. B **35**, 2923 (2013).

[6] A. Hayrapetyan, J. Götte, K. Huruntz, S. Fritzsche, and R. G. Petrosyan, Electromagnetic wave propagation in spatially homogeneous yet smoothly time-varying dielectric media, J. Quant. Spectrosc. Radiat. Transfer **178**, 158 (2016).

[7] V. Pacheco-Peña, Y. Kiasat, B. Edwards, and N. Engheta, Salient features of temporal and spatio-temporal metamaterial in *2018 International Conference on Electromagnetics in Advanced Applications (ICEAA), Cartagena, Colombia* (IEEE, 2018), pp. 524–526.

[8] J. R. Zurita-Sánchez, P. Halevi, and J. C. Cervantes-González, Reflection and transmission of a wave incident on a slab with a time-periodic dielectric function $\epsilon(t)$, Phys. Rev. A **79**, 053821 (2009).

[9] N. Wang, Z.-Q. Zhang, and C. T. Chan, Photonic Floquet media with a complex time-periodic permittivity, Phys. Rev. B **98**, 085142 (2018).

[10] T. T. Koutserimpas and R. Fleury, Electromagnetic waves in a time periodic medium with step varying refractive index, IEEE Trans. Antennas Propag. **66**, 5300 (2018).

[11] A. M. Shaltout, J. Fang, A. V. Kildishev, and V. M. Shalaev, Photonic time-crystal and momentum band-gaps, in *Conference on Lasers and Electro-Optics*, OSA Technical Digest (online), (Optical Society of America, 2016), paper FM1D.4.

[12] E. Lustig, Y. Sharabi, and M. Segev, Topological aspects of photonic time crystals, Optica **5**, 1390 (2018).

[13] J. Ma and Z.-G. Wang, Band structure and topological phase transition of photonic time crystals, Opt. Express **27**, 12914 (2019)

[14] J. S. Martínez-Romero, O. M. Becerra-Fuentes, and P. Halevi, Temporal photonic crystals with modulations of both permittivity and permeability, Phys. Rev. A **93**, 063813 (2016).

[15] N. Chamanara, Z.-L. Deck-Léger, C. Caloz, and D. Kalluri, Unusual electromagnetic modes in space-time modulated dispersion engineered media, Phys. Rev. A **97**, 063829 (2018).

[16] F. Biancalana, A. Amann, A. Uskov, and E. O'Reilly, Dynamics of light propagation in spatiotemporal dielectric structures, Phys. Rev. E **75**, 046607 (2007).

[17] S. Inampudi, M. M. Salary, S. Jafar-Zanjani, and H. Mosallaei, Rigorous space-time coupled-wave analysis for patterned surfaces with temporal permittivity modulation, Opt. Mater. Express **9**, 162 (2019).

[18] S. Taravati and G. Eleftheriades, Generalized Space-Time-Periodic Diffraction Gratings: Theory and Applications, Phys. Rev. Appl. **12**, 024026 (2019).

[19] S. Taravati and A. Kishk, Advanced wave engineering via obliquely illuminated space-time modulated slab, IEEE Trans. Antenna Propag. **67**, 270 (2019).

[20] S. Taravati, Giant Linear Nonreciprocity, Zero Reflection and Zero Band Gap in Equilibrated Space-Time-Varying Media, Phys. Rev. Appl. **9**, 064012 (2018).

[21] D. Holberg and K. Kunz, Parametric properties of fields in a slab of time-varying permittivity, IEEE Trans. Antennas Propag. **14**, 183 (1966).

[22] J. R. Zurita-Sánchez and P. Halevi, Resonances in the optical response of a slab with time-periodic dielectric function, Phys. Rev. A **81**, 053834 (2010).

[23] J. Sabino Martínez-Romero and P. Halevi, Parametric resonances in a temporal photonic crystal slab, Phys. Rev. A **98**, 053852 (2018).

[24] J. R. Zurita-Sánchez, J. H. Abundis-Patiño, and P. Halevi, Pulse propagation through a slab with time-periodic dielectric function $\epsilon(t)$, Opt. Express **20**, 5586 (2012)

[25] Y. Xiao, G. P. Agrawal, and D. N. Maywar, Spectral and temporal changes of optical pulses propagating through time-varying linear media, Opt. Lett. **36**, 505 (2011).

[26] K. Yi, M. Collet, and S. Karkar, Frequency conversion induced by time-space modulated media, Phys. Rev. B **96**, 104110 (2017).

[27] C. Qin, Z. Feng, Y. Peng, D. Sounas, X. Zhu, B. Wang, J. Dong, X. Zhang, A. Alù, and P. Lu, Spectrum Control through Discrete Frequency Diffraction in the Presence of Photonic Gauge Potentials, Phys. Rev. Lett. **120**, 133901 (2018).

[28] D. Sounas and A. Alù, Angular-momentum-biased nanorings to realize magnetic-free integrated optical isolation, ACS Photonics **1**, 198 (2014).

[29] N. A. Estep, D. Sounas, J. Soric, and A. Alù, Magnetic-free non-reciprocity and isolation based on parametrically modulated coupled resonator loops, Nat. Phys. **10**, 923 (2014).

[30] Y. Zhang, B.-K. Chen, and B.-Q. Gao, Propagation of electromagnetic waves excited by half-wave dipole antenna in time-varying media, in *2005 IEEE International Symposium on Microwave, Antenna, Propagation and EMC Technologies for Wireless Communications, Beijing, China* (IEEE, 2005), Vol. 1, pp. 318–321.

[31] K. A. Lurie and V. V. Yakovlev, Energy accumulation in waves propagating in space and time-varying transmission lines, IEEE Antennas Wireless Propag. Lett. **15**, 1681 (2016).

[32] J. R. Reyes-Ayona, and P. Halevi, Electromagnetic wave propagation in an externally modulated low-pass transmission line, IEEE Trans. Microw. Theory Tech. **64**, 3449 (2016).

[33] S. Y. Elnaggar and G. N. Milford, Modelling Space-time Periodic Structures with Arbitrary Unit Cells Using Time Periodic Circuit Theory, IEEE Trans. Antennas Propagation **68**, 6636 (2020).

[34] J. R. Reyes-Ayona and P. Halevi, Observation of genuine wave vector (k or β)gap in a dynamic transmission line and temporal photonic crystals, Appl. Phys. Lett. **107**, 074101 (2015).

[35] S. Qin and Y. E. Wang, Parametric conversion with distributedly modulated capacitors (DMC) for low-noise and non-reciprocal RF front-ends, in *2013 IEEE MTT-S International Microwave Symposium Digest (MTT), Seattle, WA, USA* (IEEE. 2013), pp. 1–3.

[36] S. Qin, Q. Xu, and Y. E. Wang, Nonreciprocal components with distributedly modulated capacitors, IEEE Trans. Microw. Theory Tech. **62**, 2260 (2014).

[37] Y. S. Li, X. P. Yu, and Z. H. Lu, Nonreciprocal time-varying transmission line with carrier boosting technique for low-noise rf front ends, IEEE Microw. Wireless Compon. Lett. **28**, 1011 (2018).

[38] W. Lee and E. Afshari, Low-noise parametric resonant amplifier, IEEE Trans. Circuits Syst. I: Reg. Papers **58**, 479 (2011).

[39] S. Taravati and C. Caloz, Mixer-duplexer-antenna leaky-wave system based on periodic space-time modulation, IEEE Trans. Antenna Propag. **65**, 442 (2017).

[40] S. Taravati, Aperiodic space-time modulation for pure frecuency mixing, Phys. Rev. B **97**, 115131 (2018).

[41] A. Shlivinski and Y. Hadad, Beyond the Bode-Fano Bound: Wideband Impedance Matching for Short Pulses Using Temporal Switching of Transmission-Line Parameters, Phys. Rev. Lett. **121**, 204301 (2018).

[42] M. Mirmoosa, G. Ptitcyn, V. Asadchy, and S. Tretyakov, Time-Varying Reactive Elements for Extreme Accumulation of Electromagnetic Energy, Phys. Rev. Appl. **11**, 014024 (2019).

[43] J. A. Richards, *Analysis of Periodically Time-Varying Systems* (Springer, Berlin, Germany, 1983).

[44] R. D. L. Krönig and W. Penney, Proc. R. Soc. Lond. A. **130**, 499 (1931).

[45] S.-H. Pan and S. M. Feng, General formalism of the Krönig-Penney model suitable for superlattice applications, Phys. Rev. B **44**, 5668 (1991).

[46] A. Esmailpour, M. Esmaeilzadeh, E. Faizabadi, P. Carpena, and M. Reza Rahimi Tabar, Metal-insulator transition in random Krönig-Penney superlattices with long-range correlated disorder, Phys. Rev. B **74**, 024206 (2006).

[47] V. Pourmahmoud and B. Rezaei, Manipulation of Bragg and graphene photonic band gaps in one-dimensional photonic crystal containing graphene, Optik **185**, 875 (2019).

[48] V. S. Proshchenko, M. Settipalli, A. K. Pimachev, and S. Neogi, Modulation of semiconductor superlattice thermopower through symmetry and strain, J. Appl. Phys. **129**, 025301 (2021).

[49] G. Luna, F. Izrailev, N. M. Makarov, U. Kuhl, and H. J. Stoeckmann, One-dimensional Krönig-Penney model with positional disorder: Theory versus experiment, Phys. Rev. B **80**, 115112 (2009).

[50] S. Mishra and S. Satpathy, One-dimensional photonic crystal: The Krönig-Penney model, Phys. Rev. B **68**, 045121 (2003).

[51] H. Hojo and A. Mase, Dispersion relation of electromagnetic waves in one-dimensional plasma photonic crystals, Plasma Fusion Res. **80**, 89 (2004).

[52] M. Bergmair and K. Hingerl, Band structure and coupled surface states in one-dimensional photonic crystals, J. Opt. A: Pure Appl. Opt. **9**, S339 (2007).

[53] S. Prasad, V. Singh, and A. Singh, Modal propagation characteristics of em waves in ternary one-dimensional plasma photonic crystals, Optik **121**, 1520 (2010).

[54] T. Mayteevarunyoo and B. Malomed, Solitons in onedimensional photonic crystals, J. Opt. Soc. Am. B **25**, 1854 (2008).

[55] T. Mayteevarunyoo, B. Malomed, and A. Roeksabutr, Solitons and vortices in nonlinear two-dimensional photonic crystals of the Krönig-Penney type, Opt. Express **19**, 17834 (2011).

[56] A. Gomez-Gomez, A. Lakhtakia, M. A. Solano, and A. Vegas, Parallel-plate waveguides with Krönig-Penney morphology as photonic band-gap filters, Microw. Opt. Technol. Lett. **36**, 4 (2003).

[57] A. Gomez-Gomez, M. A. Solano, A. Lakhtakia, and A. Vegas, Circular waveguides with Krönig-Penney morphology as photonic band-gap filters, Microw. Opt. Technol. Lett. **37**, 316 (2003).

[58] J. S. Martínez-Romero, and P. Halevi, Standing waves with infinite group velocity in a temporally periodic medium, Phys. Rev. A **96**, 063831 (2017).